SCIENCE CHINA
Earth Sciences

• RESEARCH PAPER •

December 2012 Vol.55 No.12: 2026–2038
doi: 10.1007/s11430-012-4440-1

Carbon isotopic composition of Early Triassic marine carbonates, Eastern Sichuan Basin, China

HUANG SiJing*, HUANG KeKe, LÜ Jie & LAN YeFang

State Key Laboratory of Oil/Gas Reservoir Geology and Exploitation, Institute of Sedimentary Geology, Chengdu University of Technology, Chengdu 610059, China

Received July 13, 2011; accepted November 23, 2011; published online July 13, 2012

As the interval following the biggest Phanerozoic mass extinction at the end of Permian, the Early Triassic is characterized by an immature, poorly functioned ecosystem. The effects of these extreme environmental conditions can be mirrored by the changes in the $\delta^{13}C$ record of marine carbonates. However, the details about the carbon isotopic composition and evolution of the Early Triassic seawater remain poorly understood. A dataset of new $\delta^{13}C$ and $\delta^{18}O$ values as well as selected major and trace element data (including concentrations of CaO, MgO, Mn, and Sr) was obtained from 113 marine carbonate samples collected in Eastern Sichuan Basin. The isotopic and elemental data are used to evaluate effects of thermochemical sulfate reduction on $\delta^{13}C$. The $\delta^{13}C$ values of a few samples affected by thermochemical sulfate reduction were corrected. By combining carbonate $\delta^{13}C$ results in our investigated sections, we constructed a composite curve of the Lower Triassic. The results reveal a $\delta^{13}C$ anomaly of carbonate rocks throughout the Early Triassic, accompanied by some rapid jumps and falls, such as those from approximately –2‰ to the extremely high value of 8‰ within a period of about 5 Ma. The Early Triassic $\delta^{13}C$ profile derived from Eastern Sichuan Basin shows a close correspondence with Guandao section in Guizhou Province, whereas it yields an excursion pattern differing from Chaohu section in Anhui Province of the Lower Yangtze region (with the $\delta^{13}C$ value from the minimum around –6‰ to the maximum near 4‰). The higher $\delta^{13}C$ values and the positive carbon isotope excursions in the Lower Triassic from Eastern Sichuan Basin were most likely a consequence of the principal environmental change that may include: (1) the barren land surface due to the absence of vegetation, (2) the loss of diverse marine invertebrate groups and marine carbonates, (3) the thriving of bacteria, algae and methanogenus in ocean ecosystems, and (4) the local effect of the repositories of isotopically light carbon occurred in the form of methane hydrates. This process ended at the Early-Middle Triassic boundary, which indicates that the biotic recovery started at the end of the Lower Triassic. The terrestrial vegetation and marine invertebrates, as the regulators for carbon cycle, are irreplaceable and demand strong protections.

Eastern Sichuan Basin, Early Triassic, carbon isotope, ecological destruction and reconstruction

Citation: Huang S J, Huang K K, Lü J, et al. Carbon isotopic composition of Early Triassic marine carbonates, Eastern Sichuan Basin, China. Sci China Earth Sci, 2012, 55: 2026–2038, doi: 10.1007/s11430-012-4440-1

The biggest Phanerozoic mass extinction of the past 550 million years occurred at the Permian-Triassic (P-T) boundary and witnessed the loss of about 90% or more of all marine species [1, 2]. The following Early Triassic is a period of biotic recovery. However, due to the effects of the mortality of marine organism, the dramatic loss of terrestrial vegetation and the mass extinction of marine invertebrates, the Early Triassic ecosystem is marked by extreme environmental conditions. The recovery of post-Paleozoic marine faunas did not start until the early Middle Triassic, about 5 Ma after the extinction event. This means that the reconstruction of marine ecosystems was a protracted process, lasting 5 Ma during Early Triassic.

*Corresponding author (email: hsj@cdut.edu.cn)

Many environmental and evolutionary events in Earth's history were accompanied by the global carbon cycle disturbance. Thus, carbon isotope stratigraphy is a valuable approach to elucidating the mechanisms of perturbation of ecologic environments, which may be responsible for the extinctions and recoveries. However, Early Triassic strata deposited in most parts of the earth are predominantly siliciclastic [3]. As a result, compared to relatively well-studied $\delta^{13}C$ records for other geologic timescale, the carbon isotopic data for Early Triassic are less abundant. According to previously established carbon isotope curve of the Phanerozoic (Veizer et al. [4]), only very few data points spanning the Lower Triassic are available and the isotopic profile is not continuous. The localities that have been used to report useful $\delta^{13}C$ profiles over several tens of meters above the P-T boundary include: (1) the Chaohu section in Anhui Province and the Meishan section in Zhejiang Province [5] (Figure 1) and (2) marine settings of Italy, Hungary, Slovakia, Germany and Iran [6–8]. The entirety of the interval spanning the Lower Triassic, however, is lacking, due to the paucity of samples through part of Smithian and Spathian sub-stages (Figure 2) [8–10]. Besides, Horacek et al. [11] used systematically sampled complete sections in Northern Italy to establish a continuous carbon isotope curve of Early Triassic seawater (Figure 3). Payne et al. [12] provided relatively high-resolution datasets from three sections in Guizhou Province, China. However, only Guandao section spans the Lower Triassic in its entirety, which is composed of the Griesbachian, Dinerian, Smithian, and Spathian sub-stages, respectively (Figure 4). Here, we review the currently available carbon isotope data and suggest that:

(1) In view of the absence of the perfect proxies for ancient seawater samples, such as brachiopod shells, previous studies of carbon isotopic evolution of Early Triassic were largely carried out through whole-rock analysis of carbonates that have precipitated from coeval seawater. Although some measurements have been obtained from brachiopod shells [6], the samples are not from Early Triassic (Figure 2(b)). Further, some authors choose dolomites as proxies for seawater samples and show that the $\delta^{13}C$ did not change significantly during dolomitization [11, 12].

(2) At the locality of Luodian of Guizhou Province, South China, carbon isotope data outlined a positive excursion at the Dienerian-Smithian boundary, reaching the highest value at 6‰ from Guandao section (Figure 4) and 8‰ from two adjacent sections. Such Spathian-Anisian positive carbon isotope shift was also reported for Uomo

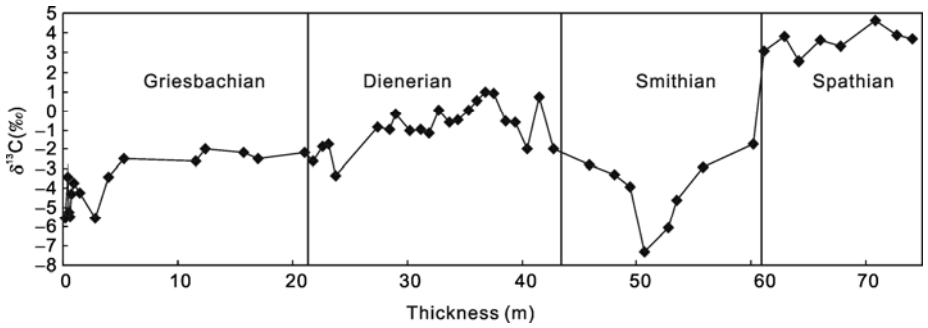

Figure 1 Carbon isotope curves derived from Lower Triassic carbonate rocks from Beipo section in Chaohu, Anhui Province, China (after ref. [5]).

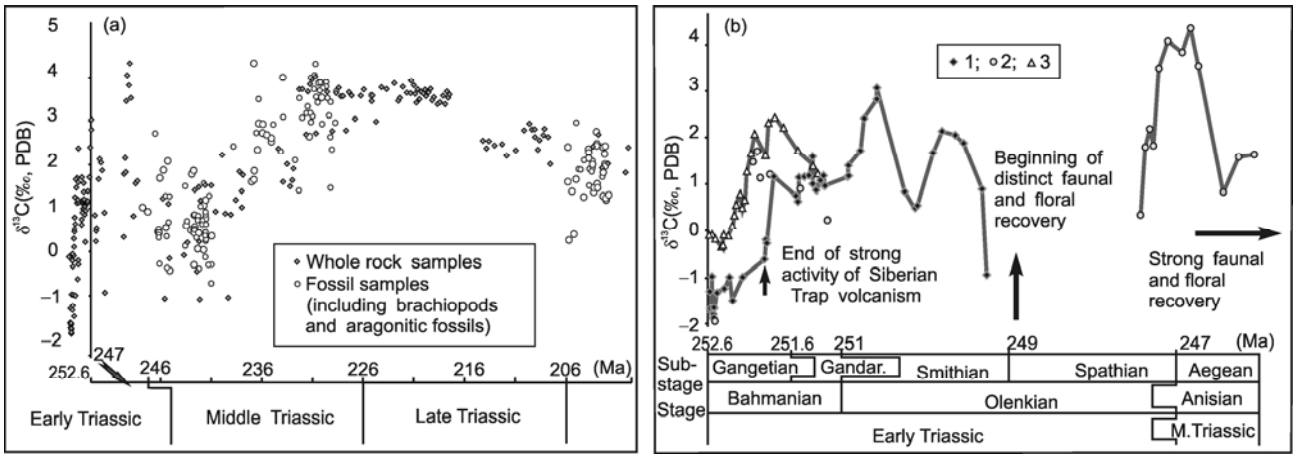

Figure 2 Carbon isotope evolution curve of Triassic seawater [6–8] (a) and an expansion of the part of the Early Triassic (b). Absolute ages are based on refs. [9, 10]. 1. whole rock samples (Pufels, Southern Alps, from refs. [6, 8]); 2. whole rock samples (Palazzo Adriano, Sicily, from ref. [6]); 3. whole rock samples (Abadeh, Iran, from ref. [7]).

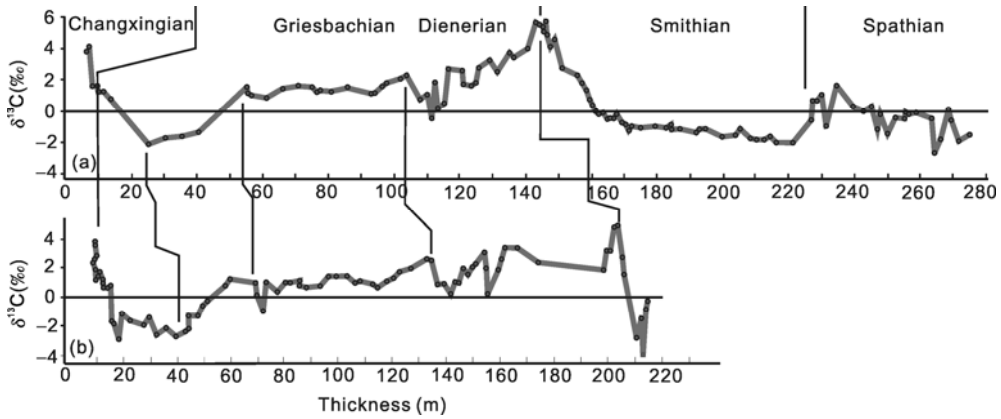

Figure 3 Carbon isotope evolution curve of Late Permian to Early Triassic of Uomo section (a) and Pufels section (b), northern Italy (from ref. [11]).

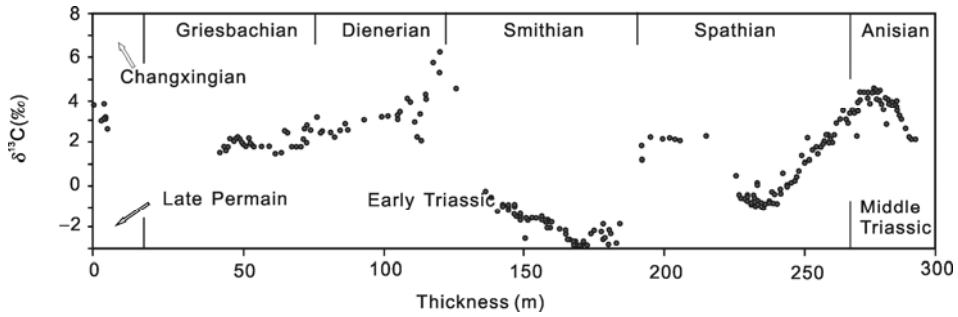

Figure 4 Carbon isotope evolution curve for marine carbonates of Guandao section, Guizhou Province, China (from ref. [12]).

section in Northern Italy with the peak carbon isotope value of about 6‰ (Figure 3). However, coeval samples from Alps and Iran [6] show distinctly lower shift values with the positive peak of less than 4.5‰, which are situated close to the Early-Middle Triassic boundary (Figure 2). A moderate positive excursion was obtained for Beipo section in the middle part of Anhui Province and its excursion peak occurs within the Spathian of value around 5‰ (Figure 1). Therefore, the Early Triassic carbon isotope curve differs remarkably among the previously investigated sections, and it is difficult to define a general carbon isotope trend for the Early Triassic interval.

(3) In particular, the Early Triassic $\delta^{13}C$ values from the Lower Yangtze sections are much lower than those from elsewhere. For instance, the $\delta^{13}C$ values from the Beipo section are less than 0 within Griesbachain sub-stage, whereas those are more than 0 from many other regions (e.g., Guandao section [12]).

Overall, since the Upper Permian and the Lower Triassic in most parts of the world are represented by siliciclastic deposits, the published $\delta^{13}C$ data of the Lower Triassic are very limited and therefore the changes in the carbon cycle during the Lower Triassic are poorly understood. Furthermore, the $\delta^{13}C$ curve from each section shows a distinct trend throughout the Early Triassic. These findings raise the question of whether the published carbon isotope curves for the Lower Triassic represent a global pattern or just a regional signal. If the latter is true, then the samples may not represent original seawater carbon isotopic signature. In fact, in most studies, samples were evaluated for their reliability as proxies of original seawater carbon. For instance, Tong et al. [5] and Zuo et al. [13] reported that there was no correlation between carbon- and oxygen-isotope values, proving the absence of significant diagenetic alteration of the rocks, though the samples contain high magnesium contents, low strontium contents, and high Mn/Sr ratio. Thus, there is some confusion over the reliability of the stratigraphic correlation by carbon isotope curves. This will arouse our greater curiosity in obtaining the carbon isotopic values for the Lower Triassic seawater.

In order to detect detailed changes in $\delta^{13}C$ record of seawater after the Permian-Triassic boundary event, this paper describes and interprets the carbon isotopic compositions of Lower Triassic carbonates of the Eastern Sichuan Basin. The results are also compared to profiles from other investigated regions.

1 Geological setting and sampling

Carbon isotopic samples were collected from three sections and one well in Eastern Sichuan Basin, China. Zhongliang Mountain section and Beibei section are exposed in Chongqing area, and Yangtianwo section and Well Heba-1 are

located in Eastern Sichuan Basin (Figure 5). The carbonate succession of studied area is lithologically divided into four units, starting from the Late Permian Changxing Formation (P_2c), through the P-T boundary (P/T) into the Feixianguan (T_1f), Jialingjiang Formation (T_1j) of Early Triassic and Leikoupo Formation (T_2l) of Middle Triassic. A continuous Late Permian Changxing Formation and P-T succession is well exposed at Zhongliangshan section, and the Triassic sequence, including Feixianguan, Jialingjiang and Leikoupo Formation, is located at Yangtianwo section. Lithologically, the 2nd and 4th Members of Jialingjiang Formation (T_1j^2 and T_1j^4) at Yangtianwo section are composed mainly of dolomites and evaporates. For this, the samples from Beibei section have been selected as the supplement for the T_1j^2 sequence and core samples of the T_1j^4 dolomite strata were collected from Well Heba-1. The above three sections are located in the northeast of a broom-like belts in Huaying Mountain. Well Heba-1 is located in the joint of the Daba Mountains fold belt and the northeast of Huaying Mountain broom-like belts (Figure 5).

As described above, we are unable to provide a continuous carbon isotope profile over the required timescale from a single section. However, by means of synchronous lithological markers, it is possible to construct a composite $\delta^{13}C$ profile by piecing the data from different sections/wells together: (1) selecting the P-T boundary as joint, by which the $\delta^{13}C$ profile of Zhongliangshan section and Yangtianwo section could be compiled; (2) assuming the deposition rate is constant over T_1j^4 period, it is reasonable to converse vertical thickness into horizontal thickness proportionally, then the profile could be aided by additional data from Well Heba-1; (3) in this manner, a few data from Beibei section can also be incorporated into composite $\delta^{13}C$ curves. Data from different sections or wells plotted in all figures are distinguished by different symbols.

Permian-Triassic boundary is well exposed in Zhongliangshan section, where the boundary could be easily identified lithologically: the top of the Permian Changxing Formation consists of bioclastic-bearing microcrystalline limestone with chert concretions, whereas the Triassic Feixianguan Formation is mainly fuchsia argillaceous microcrystalline limestone (Figure 6). This boundary layer is about 1 m in thickness and contains at least three grey clay beds, which have been identified by geochemical and petrographic analysis as volcanic ash beds. Such P-T boundary clay beds are widespread in South China, such as Meishan section in Changxing, Zhejiang Province and Shangsi section in Guangyuan, Sichuan Province. These clays are usually dominated by mixed-layer illite/smectite [14], with euhedral zircon, euhedral hexagonal bipyramid quartz and volcanic pellets [15].

2 Analytical techniques

Hand specimens collected from the localities of Eastern Sichuan Basin described above were critically investigated for veins and strong recrystallization. These samples were crudely crushed and carefully handpicked to winkle the calcite veins and sparry cements as much as possible, and then were crushed into powder (<200 mesh) and divided into three splits, one for backup, and the other two for element analysis and C, O and Sr isotope determinations, respectively. Calcite and dolomite content of the samples were calculated from the measured CaO and MgO values. Petrographic observations were also carried out with polished thin sections, some of which were stained by Alizarin Red-S. These thin sections were also used for cathodoluminescence (CL) analysis, and most samples show no luminescence or dull luminescence, which may be caused by lower Mn concentration [16].

Carbon and oxygen isotope composition of samples were accomplished at Research Institute of Exploration and Development, Southwestern Oil and Gasfield Branch Company, PetroChina. They were measured in a Finnigan MAT

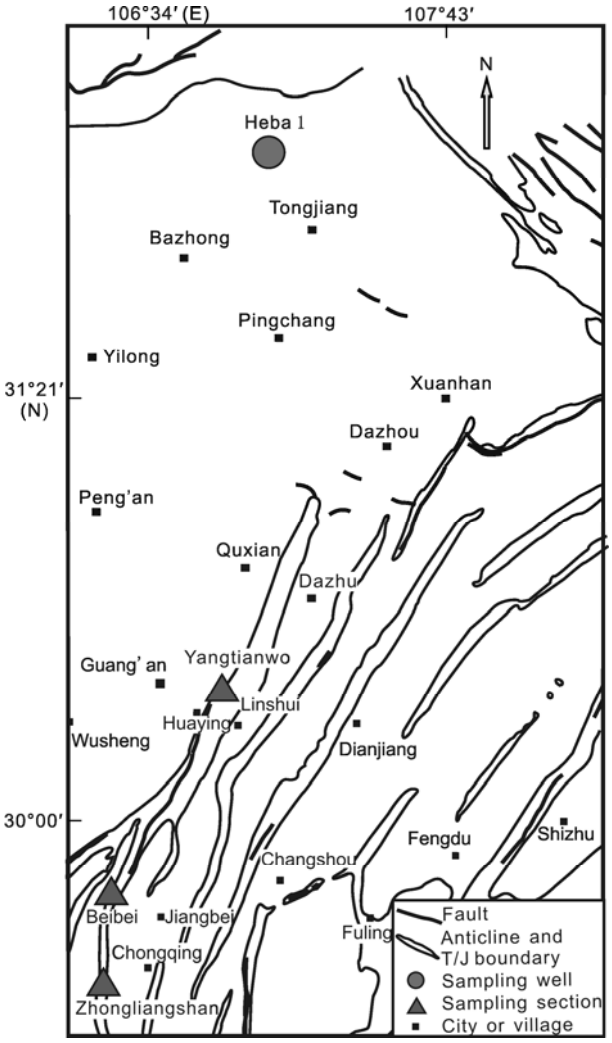

Figure 5 Geological map showing sampling sections and wells. Modified from 1∶100000 geological map of Sichuan Province.

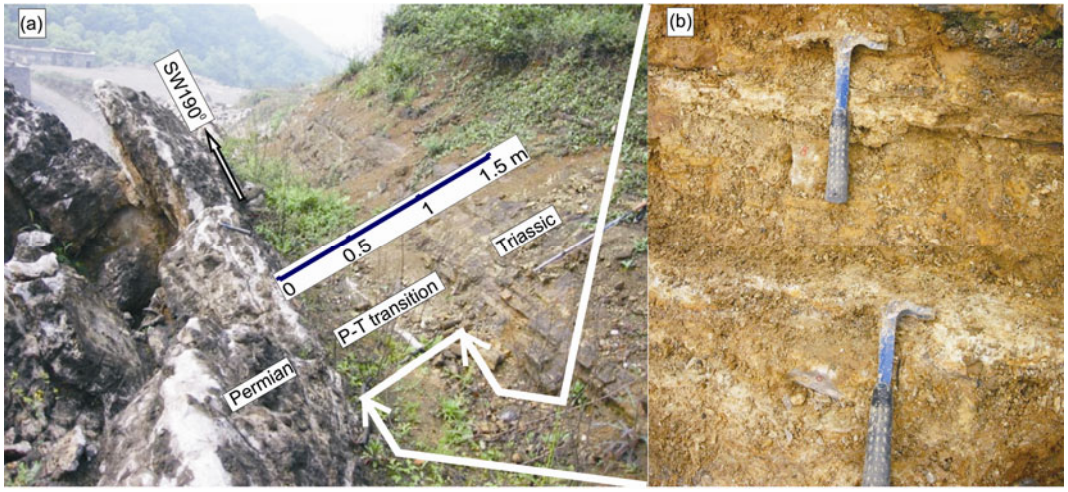

Figure 6 The Permian-Triassic boundary interval in the Zhongliangshan section of China. (a) Photomicrographs showing the significant differences in lithology between the Upper Permian and the Lower Triassic strata; (b) amplified image of the P-T boundary showing the presence of three grey clay beds.

252 mass spectrometer and reported in the $\delta^{13}C$ and $\delta^{18}O$ notation relative to the PDB standard. Precision is on the order of 0.01‰ for $\delta^{13}C$ and $\delta^{18}O$. Two major element oxides (CaO and MgO) were analyzed using volumetric analysis method with 1% detection limit and 5% error; two trace elements (Mn, Sr) were determined by atomic absorption spectrophotometer with the testing limits of 5 and 42 ppm, and errors of 13% and 14%, respectively. These analyses were carried out at Geological and Mineralogical Testing Center of Huayang in Sichuan Province. CL observation was under the Leica microscope using CL8200MK5 luminoscope system. Operating conditions were mean 12 kV and 300 μA.

3 Results

A total of 116 bulk samples were analyzed for their oxygen- and carbon-isotope compositions. The concentrations of CaO, MgO, Mn and Sr were also obtained from 110 out of these 116 samples, which are used to evaluate preservation potential of original seawater carbon (Table 1). The strontium isotopic results of 73 samples listed in Table 1 have been previously published by Hu et al. [17] and Huang et al. [18].

3.1 Mn, Sr contents and Mn/Sr ratios

The stable isotopic composition of sediments might be modified by diagenetic alteration. Because of this, evaluating the effects of diagenesis on the isotopic compositions is very important. Diagenetic alteration of marine carbonates tends to increase the Mn content and decrease the Sr content in carbonates [16, 19], so the analysis of Mn and Sr contents can provide insight into whether the carbonate samples represent seawater information [3, 20, 21]. The results (Table 1) exhibit relatively high Sr concentrations: 73 samples contain more than 250 ppm Sr with an average of 636 ppm and up to a maximum value of 2613 ppm. Due to the lower Sr distribution coefficient for dolomites [22], the samples with Sr concentration lower than 250 ppm are dolomites (MgO concentrations larger than 15%). So, most samples are higher than the minimum Sr concentration (200 ppm) for strontium-isotope stratigraphy (SIS) research suggested by Derry et al. [23] and can be selected to study the SIS. However, there are nine samples with Mn/Sr ratio higher than 2. According to Kaufman et al. [24, 25], samples of the Mn/Sr ratio above 2–3 should be treated as altered and must not be used for reconstruction of seawater composition. Therefore, the isotopic values of these nine samples should be excluded from further discussion. In addition, it is known that the amount of manganese is necessary to induce luminescence in carbonates and the amount of ferrous iron is necessary to quench manganese-induced luminescence. Thus, most of our samples show no luminescence or dull luminescence, and they are not stained by potassium ferricyanide. This suggests the relatively low Mn concentrations in the samples. In conclusion, our studied samples have higher concentrations of Sr and lower amounts of Mn and can be used as proxies for coeval seawater.

3.2 Oxygen isotope composition

The oxygen isotopic composition of carbonate rocks is likely to be highly susceptible to diagenetic alteration [5, 26]. Thus, the lack of correlation between carbon- and oxygen-isotope indicates the carbon isotope composition was not affected during diagenetic alteration and could be seen as pristine (Figure 7(a)). Samples with higher dolomite contents show relatively high $\delta^{18}O$ values, while the $\delta^{13}C$ values of these samples are close to their less-dolomite-content neighbor samples and to the overall profile. Similar

Table 1 The $\delta^{13}C$ and $\delta^{18}O$ values, CaO, MgO, Mn and Sr concentrations and $^{87}Sr/^{86}Sr$ ratios for sections at Eastern Sichuan Basin

Section/well	Horizon	Accumulative thickness (m)	CaO (%)	MgO (%)	Mn (ppm)	Sr (ppm)	Mn/Sr	$\delta^{13}C$ (‰)	$\delta^{13}C$(‰)[a)]	$\delta^{18}O$ (‰)	$^{87}Sr/^{86}Sr$	Remark
Zhongliang Mountain	P_2c	1.0						4.05		–6.34		
Zhongliang Mountain	P_2c	7.0						3.77		–6.73		
Zhongliang Mountain	P_2c	15.5						4.51		–7.24		
Zhongliang Mountain	P_2c	17.0	44.02	1.64	78.0	1278.0	0.06	3.99		–6.22	0.707061	
Zhongliang Mountain	P_2c	27.0	53.58	1.10	105.0	1620.0	0.06	3.95		–5.34	0.707011	
Zhongliang Mountain	P_2c	31.0						3.50		–6.90		
Zhongliang Mountain	P_2c	36.0	52.00	3.55	36.0	1525.4	0.02	3.80		–-6.31		
Zhongliang Mountain	P_2c	37.0	54.86	0.51	52.0	1659.0	0.03	4.40		–6.63	0.707053	
Zhongliang Mountain	P_2c	43.5	54.85	0.75	35.4	1875.6	0.02	3.35		–6.91		
Zhongliang Mountain	P_2c	46.0	57.48	0.43	27.9	1592.7	0.02	3.22		–5.85		
Zhongliang Mountain	P_2c	49.0						3.20		–6.93		
Zhongliang Mountain	P_2c	50.0	51.82	2.70	45.0	1000.0	0.05	3.69		–7.07	0.707075	
Zhongliang Mountain	P_2c	54.8	53.77	0.28	39.0	1045.0	0.04	2.66		–5.74	0.707081	
Zhongliang Mountain	P_2c	55.6	50.47	0.28	67.0	1650.0	0.04	2.61		–6.13	0.707105	
Zhongliang Mountain	P_2c	56.4	45.83	0.56	77.0	1410.0	0.05	2.29		–6.26	0.707048	
Zhongliang Mountain	P_2c	57.2	44.64	0.38	282.0	1425.0	0.20	1.51		–7.29	0.707111	
Zhongliang Mountain	P/T	58.2	48.61	0.18	369.0	1550.0	0.24	1.09		–7.67	0.70713	
Zhongliang Mountain	P/T	58.4	50.47	0.48	479.0	1130.0	0.42	–0.94		–7.37	0.707123	
Zhongliang Mountain	P/T	58.5	48.22	0.66	471.0	980.0	0.48	0.00		–7.04	0.707122	
Zhongliang Mountain	P/T	58.5	0.63	0.04	485.1	92.2	5.26	2.62		–8.40		winkled
Zhongliang Mountain	P/T	58.8	27.82	0.76	393.0	625.0	0.63	0.01		–7.73	0.707189	
Zhongliang Mountain	P/T	59.0	43.31	0.28	628.0	910.0	0.69	–0.26		–7.53	0.707141	
Zhongliang Mountain	P/T	59.1	39.60	0.56	670.0	1410.0	0.48	–0.43		–9.86	0.707176	
Zhongliang Mountain	P/T	60.6	31.26	2.95	565.0	510.0	1.11	–1.26		–7.74	0.707085	
Yangtianwo	T_1f	61.6	44.10	1.72	2354.0	291.0	8.09	–0.04		–5.57	0.707227	winkled
Yangtianwo	T_1f	62.9	19.31	4.01	1367.0	470.0	2.91	–3.04		–6.76	0.707418	winkled
Yangtianwo	T_1f	65.7	36.98	3.00	108.0	920.0	0.12	–1.25		–6.11	0.70721	
Yangtianwo	T_1f	68.2	35.82	1.84	794.0	900.0	0.88	–1.59		–5.95	0.707216	
Yangtianwo	T_1f	73.4	33.02	2.34	635.0	1035.0	0.61	–1.08		–6.07	0.707253	
Yangtianwo	T_1f	77.4	35.82	0.99	999.0	1120.0	0.89	–1.05		–6.25	0.707219	
Yangtianwo	T_1f	93.4	33.02	2.67	523.0	1360.0	0.38	0.12		–6.04	0.707217	
Zhongliang Mountain	T_1f	104.0						–1.14		–6.76		
Yangtianwo	T_1f	123.9	39.77	2.01	418.0	1396.0	0.30	0.49		–6.19	0.70719	
Yangtianwo	T_1f	143.9	47.45	1.51	182.0	2415.0	0.08	0.30		–5.85	0.707211	
Yangtianwo	T_1f	167.0	50.23	0.50	325.0	1015.0	0.32	1.05		–5.39	0.707245	
Yangtianwo	T_1f	185.9	50.47	0.83	97.0	625.0	0.16	1.81		–5.05	0.707277	
Yangtianwo	T_1f	211.3	52.56	0.50	101.0	985.0	0.10	2.29		–5.62	0.707265	
Yangtianwo	T_1f	231.0	43.95	1.51	259.0	765.0	0.34	1.98		–5.63	0.707302	
Yangtianwo	T_1f	252.7	50.01	0.66	236.0	815.0	0.29	2.42		–5.82	0.70729	
Yangtianwo	T_1f	269.7	50.23	1.18	112.0	875.0	0.13	2.33		–5.40	0.707295	
Yangtianwo	T_1f	294.7	37.68	3.00	387.0	705.0	0.55	1.74		–5.29	0.707308	
Yangtianwo	T_1f	319.2	46.97	1.34	329.0	1050.0	0.31	2.15		–5.69	0.707309	
Yangtianwo	T_1f	333.7	11.87	2.67	968.0	250.0	3.87	–2.61		–6.22	0.707667	winkled
Yangtianwo	T_1f	349.7	24.18	2.17	848.0	310.0	2.74	–0.14		–5.79	0.707516	winkled
Yangtianwo	T_1f	379.8	51.40	0.73	349.0	480.0	0.73	0.94		–5.59	0.707327	
Yangtianwo	T_1f	380.1	54.13	0.90	290.0	2613.0	0.11	1.19		–5.21	0.707297	
Yangtianwo	T_1f	380.3	52.08	1.14	256.0	602.0	0.43	1.31		–5.58	0.707316	
Yangtianwo	T_1f	380.4	51.40	2.04	267.0	603.0	0.44	1.29		–5.43	0.707346	
Yangtianwo	T_1f	380.6	53.68	1.39	225.0	592.0	0.38	1.19		–5.51	0.707331	
Yangtianwo	T_1f	381.0	50.48	1.31	248.0	485.0	0.51	1.48		–5.81	0.707312	
Yangtianwo	T_1f	381.4	54.36	3.43	294.0	417.0	0.71	1.41		–5.86	0.707327	

(*To be continued on the next page*)

(*Continued*)

Section/well	Horizon	Accumulative thickness (m)	CaO (%)	MgO (%)	Mn (ppm)	Sr (ppm)	Mn/Sr	δ^{13}C (‰)	δ^{13}C(‰)[a)]	δ^{18}O (‰)	^{87}Sr/^{86}Sr	Remark
Yangtianwo	T_1f	385.2	53.03	0.50	108.0	655.0	0.16	1.30		–5.64	0.707373	
Yangtianwo	T_1f	424.7	53.72	1.34	8.0	530.0	0.02	1.28		–5.47	0.707474	
Yangtianwo	T_1f	441.2	52.79	0.83	50.0	1310.0	0.04	2.22		–5.69	0.707514	
Yangtianwo	T_1f	465.2	54.66	1.51	23.0	560.0	0.04	2.99		–5.72	0.707506	
Yangtianwo	T_1f	489.2	54.66	0.17	8.0	745.0	0.01	3.05		–5.74	0.707554	
Yangtianwo	T_1f	510.2	49.31	0.99	182.0	750.0	0.24	3.76		–5.66	0.707614	
Yangtianwo	T_1f	529.9	51.40	0.33	85.0	735.0	0.12	3.45		–5.47	0.707614	
Yangtianwo	T_1f	562.9	49.30	0.83	259.0	620.0	0.42	3.92		–5.67	0.707675	
Yangtianwo	T_1j^1	577.0	45.81	1.51	325.0	270.0	1.20	4.88		–5.26	0.707749	
Yangtianwo	T_1j^1	595.0	53.49	0.33	97.0	665.0	0.15	4.69		–5.38	0.707753	
Yangtianwo	T_1j^1	619.0	50.01	1.34	77.0	525.0	0.15	2.28		–5.55	0.707788	
Yangtianwo	T_1j^1	638.0	52.56	0.50	35.0	910.0	0.04	0.74		–5.62	0.707785	
Yangtianwo	T_1j^1	658.0	53.72	0.33	39.0	1190.0	0.03	–0.10		–5.83	0.707799	
Heba 1	T_1j^2	680.8	26.13	18.64	296.7	1413.0	0.21	–0.49		–3.98		
Heba 1	T_1j^2	685.4	26.33	19.14	263.3	117.5	2.24	–0.06		–3.67		winkled
Heba 1	T_1j^2	692.2	28.69	18.13	137.9	480.2	0.29	1.08		–3.71		
Heba 1	T_1j^2	698.1	26.91	18.58	187.4	305.5	0.61	2.08		–3.88		
Heba 1	T_1j^2	701.8	23.43	18.03	167.2	151.4	1.10	0.84		–4.12		
Heba 1	T_1j^2	707.9	26.37	18.89	154.3	163.7	0.94	1.49		–4.35		
Yangtianwo	T_1j^2	710.5	37.21	7.86	174.0	430.0	0.40	–1.47		–4.41	0.707996	
Heba 1	T_1j^2	710.9	30.19	15.82	132.5	935.2	0.14	1.61		–4.12		
Heba 1	T_1j^2	739.1	6.54	10.30	286.6	347.8	0.82	–1.07		–3.24		
Yangtianwo	T_1j^2	750.5	34.42	17.54	89.0	120.0	0.74	2.94		–3.62	0.708339	
Heba 1	T_1j^2	752.0	34.10	16.90	32.0	253.4	0.13	7.36		–3.92		
Heba 1	T_1j^2	753.4	33.46	19.83	70.8	154.4	0.46	6.32	8.01	–4.16		
Heba 1	T_1j^2	754.0	29.71	20.56	27.1	113.6	0.24	6.84	7.15	–3.59		
Heba 1	T_1j^2	755.1	30.14	20.91	26.1	87.2	0.30	7.02	7.32	–2.79		
Heba 1	T_1j^2	756.5	34.91	18.01	13.1	367.4	0.04	2.52	5.57	–4.36		
Heba 1	T_1j^2	759.0	29.12	20.51	29.5	86.6	0.34	6.50	6.68	–3.14		
Heba 1	T_1j^2	759.0	32.62	20.02	58.5	104.3	0.56	5.72	7.07	–4.02		
Heba 1	T_1j^2	759.0	32.62	20.02	58.5	104.3	0.56	5.72	7.07	–4.02		
Heba 1	T_1j^2	759.6	29.89	20.73	22.8	95.1	0.24	6.33	6.63	–3.31		
Heba 1	T_1j^2	760.3	31.94	19.23	27.9	193.9	0.14	5.44	6.91	–4.21		
Heba 1	T_1j^2	762.2	30.02	21.01	23.7	97.4	0.24	5.99	6.22	–3.21		
Heba 1	T_1j^2	763.4	30.48	20.56	17.7	126.3	0.14	5.76	6.28	–3.50		
Heba 1	T_1j^2	763.4	30.78	20.64	11.9	140.4	0.08	5.62	6.19	–3.40		
Heba 1	T_1j^2	763.4	30.96	20.26	27.6	156.2	0.18	5.35	6.12	–3.81		
Heba 1	T_1j^2	763.7	30.64	20.33	24.5	135.5	0.18	5.21	5.86	–3.70		
Heba 1	T_1j^2	763.7	32.96	18.98	22.2	224.3	0.10	4.23	6.14	–3.90		
Heba 1	T_1j^2	767.0	33.88	18.66	17.3	384.8	0.05	1.57	3.93	–4.04		
Yangtianwo	T_1j^3	767.5	38.13	0.83	46.0	210.0	0.22	–0.38		–5.93	0.70813	
Yangtianwo	T_1j^3	783.5	53.03	1.51	31.0	1310.0	0.02	0.29		–5.17	0.70811	
Yangtianwo	T_1j^3	805.5	49.07	0.66	70.0	585.0	0.12	0.06		–5.42	0.708126	
Yangtianwo	T_1j^3	823.5	50.70	1.34	31.0	235.0	0.13	–0.30		–5.57	0.708126	
Yangtianwo	T_1j^3	853.5	51.17	0.66	39.0	770.0	0.05	–0.27		–5.40	0.708158	
Yangtianwo	T_1j^4	888.5	30.46	19.05	58.0	35.0	1.66	–1.34		–3.50	0.708428	
Yangtianwo	T_1j^4	908.4	28.38	19.39	50.0	90.0	0.56	0.03		–3.71	0.708322	
Yangtianwo	T_1j^4	939.4	31.86	18.89	58.0	100.0	0.58	2.23		–4.70	0.708286	
Yangtianwo	T_1j^4	950.8	28.66	21.23	122.9	88.9	1.38	–0.92		–5.11		
Beibei	T_1j^4	951.0	31.01	20.75	86.6	77.5	1.12	0.38		–3.79		
Yangtianwo	T_1j^4	954.4	46.75	0.17	4.0	1015.0	0.00	1.57		–4.87	0.708208	

(*To be continued on the next page*)

(*Continued*)

Section/well	Horizon	Accumulative thickness (m)	CaO (%)	MgO (%)	Mn (ppm)	Sr (ppm)	Mn/Sr	δ^{13}C (‰)	δ^{13}C(‰)[a)]	δ^{18}O (‰)	^{87}Sr/^{86}Sr	Remark
Beibei	T_1j^4	961.5	32.57	20.12	85.7	93.2	0.92	–0.46		–3.94		
Yangtianwo	T_1j^4	964.0	30.44	24.24	100.2	65.7	1.53	–1.72		–3.99		
Zhongliang Mountain	T_1j^4	971.9	29.59	18.40	177.5	71.2	2.49	–0.32		–5.75		winkled
Yangtianwo	T_1j^4	974.2	29.02	26.50	63.3	84.8	0.75	0.69		–3.56		
Zhongliang Mountain	T_1j^4	993.6	35.76	15.27	178.2	136.7	1.30	–1.61		–7.23		
Beibei	T_1j^4	1013.1	50.06	0.45	97.1	244.5	0.40	–1.56		–8.35		
Yangtianwo	T_2l	1028.4	26.74	18.22	306.0	95.0	3.22	–1.46		–0.88	0.709252	winkled
Yangtianwo	T_2l	1045.4	30.00	18.22	151.0	75.0	2.01	–1.00		–2.56	0.708222	winkled
Yangtianwo	T_2l	1160.4	45.11	1.67	85.0	255.0	0.33	–0.73		–3.75	0.708083	
Yangtianwo	T_2l	1180.4	41.17	1.84	97.0	65.0	1.49	–0.79		–3.73	0.70806	
Yangtianwo	T_2l	1210.4	51.40	0.17	128.0	210.0	0.61	0.76		–5.52	0.707981	
Yangtianwo	T_2l	1240.4	49.53	0.66	147.0	540.0	0.27	1.70		–6.62	0.708076	
Yangtianwo	T_2l	1247.4	46.97	3.00	93.0	280.0	0.33	1.03		–4.84	0.708043	
Yangtianwo	T_2l	1257.4	54.36	0.98	143.0	128.0	1.12	0.98		–7.72	0.707872	

a) In case of samples show "TSR" signatures, correction of δ^{13}C value is indicated.

results at Northern Italy were given by Horacek et al. [11], which suggested that evaporative brine would cause the ^{18}O enrichment of dolomite samples but would not affect the δ^{13}C values of those samples. Thus, the δ^{13}C values of these dolomite samples are likely to preserve the original seawater δ^{13}C signal.

During diagenetic process, the whole rock samples rich in carbonate minerals have a higher potential to preserve their initial carbon isotope compositions than oxygen isotope compositions. This is because the amount of diagenetically transported CO_2 is normally far outmatched by the amount of carbon present in the wall rock. In most cases, diagenetic process, except for bacterial methanogenesis [27], might produce depletion in δ^{13}C values. This indicates that the larger amount of organic carbon can be provided during the burial. The source of organic carbon in the samples from our studied sections is very limited and does not seem to significantly change the carbonate δ^{13}C composition. Thus, the δ^{13}C values of these samples primarily reflect inheritance of marine carbon. However, the samples taken from Well Heba-1 often comprise TSR-originated calcite cements, which potentially might influence the δ^{13}C composition of whole rock samples. Hence, isotopic analyses of bulk samples cannot provide exact information of seawater and an appropriate method should be applied to correct the δ^{13}C values.

3.3 Correction of δ^{13}C values

The samples taken from Well Heba-1 are primarily silty to fine crystalline dolomites (Figure 8) and the dolomitization of these samples is believed to be promoted by coeval seawater [28]. Because of this, they can be served as useful proxies for seawater. However, these dolomites contain abundant calcite cements as products of TSR [29], which yield high homogenization temperature values ranging from

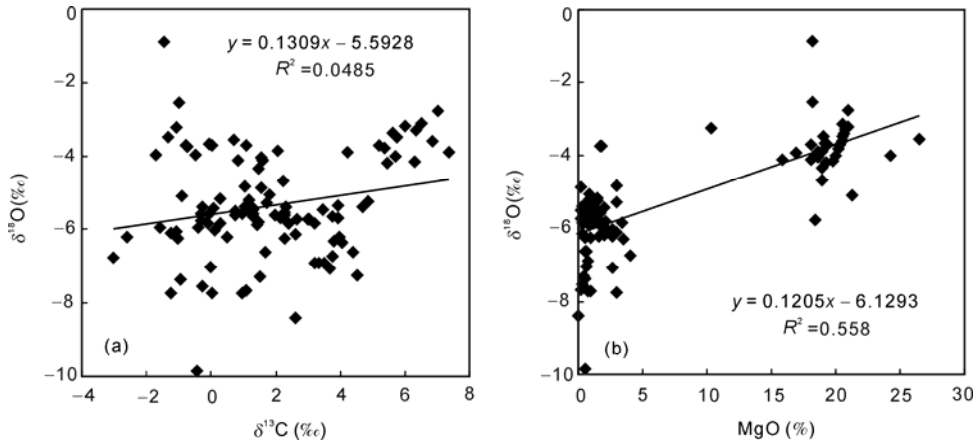

Figure 7 Cross-plots of δ^{18}O values vs δ^{13}C values (a) and of δ^{18}O values vs MgO concentrations (b).

110 to 140°C. In order to investigate the effect of TSR on the isotopic compositions of carbon and oxygen, the $\delta^{13}C$ and $\delta^{18}O$ composition data of these samples are plotted against the amounts of calcite cements (Figure 9). Clearly, there is a negative correlation between the $\delta^{13}C$ values and the calcite contents, and between the $\delta^{18}O$ values and the calcite contents, suggesting that the variations of $\delta^{13}C$ values of these samples can be formulated as a function of calcite percentage. Due to sampling depth interval spanning only 5.8 m, the age effect on isotope record could be ignored. Therefore, the $\delta^{13}C$ values can be corrected by assuming samples with a composition of 100% dolomite and the calculated results are listed in Table 1. More detailed discussions are available from reference [29].

All calcites occur in fine-silty crystalline dolomites. Dolomites are euhedral-subhedral crystal. The scattered blue is cast resin. Well Heba-1, 2nd Member, Jialingjiang Formation, Triassic, Eastern Sichuan Basin, China. The diagonal line is 1.5 mm for photo (a) and 0.75 mm for photo (b).

4 Discussions

4.1 The ages of P-T boundary and Early-Middle Triassic boundary and their global correlation

(1) The P-T boundary. The P-T boundary itself can be easily identified lithologically in the sections of southern China (Figure 6), and it commonly occurs in claystones as the result of volcanic ash alteration. U-Pb analyses on single zircon crystals have been applied by using SHRIMP for dating volcanic ash layers within the P-T boundary at Meishan and Shangsi sections [30, 31], which define an age of 252.6±0.2 Ma. A dramatic negative shift of $\delta^{13}C$ associated with the P-T boundary has been widely recognized [5, 13, 32–35] and also reproduced in the carbon isotopic profiles showed in Figure 10(a) and 10(b), relying on the age of the P-T boundary of 252.6 and 251.4 Ma, respectively.

(2) The Early-Middle Triassic boundary. The Triassic carbonates or evaporates are well exposed at many sections in Southwestern China, where the Early-Middle Triassic boundary beds commonly occur as altered tuff and siliceous shale (locally called "green-bean rock"). This boundary, as demonstrated by the synchronous volcanic event control, is customarily used as a mapping unit to separate the Lower from Middle Triassic marine rocks in South China. For these, the green-bean rock is Early-Middle Triassic boundary in this study (Figure 10(a)). Wang et al. [36] applied U-Pb analyses on zircon crystals to date the volcanic ash layers of Early-Middle Triassic boundary from Ganheqiao section in Guizhou Province, southern China and define a $^{206}Pb/^{238}U$ age of 239.0±2.9 Ma. Similar age data of 241.9 Ma, provided by Huang et al. [41], are measured by Stron

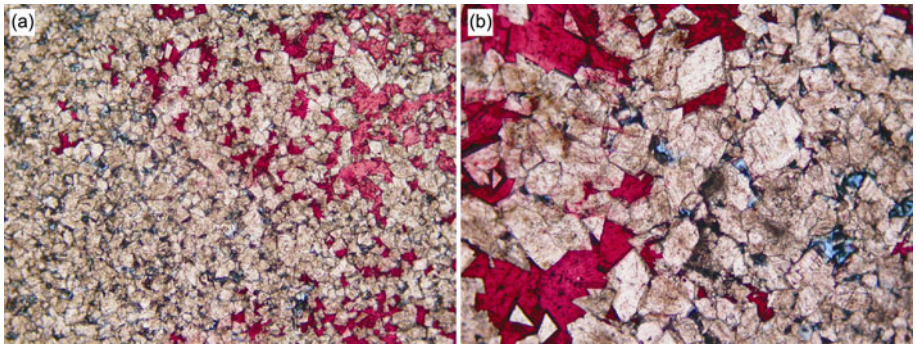

Figure 8 Thin section photomicrographs (plain light) of the TSR calcite cements (stained by Alizarin Red-S).

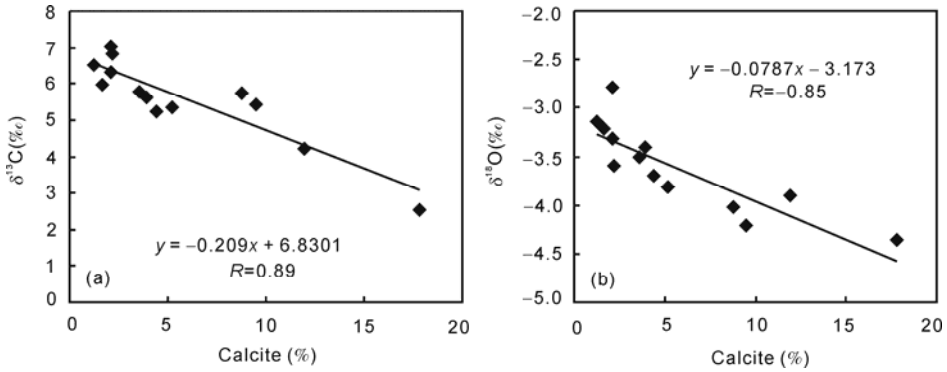

Figure 9 Plots of $\delta^{13}C$, $\delta^{18}O$ vs calcite content in fine-silty crystalline dolomites. All samples are taken from Well Heba-1, and depth interval is 5.8 m.

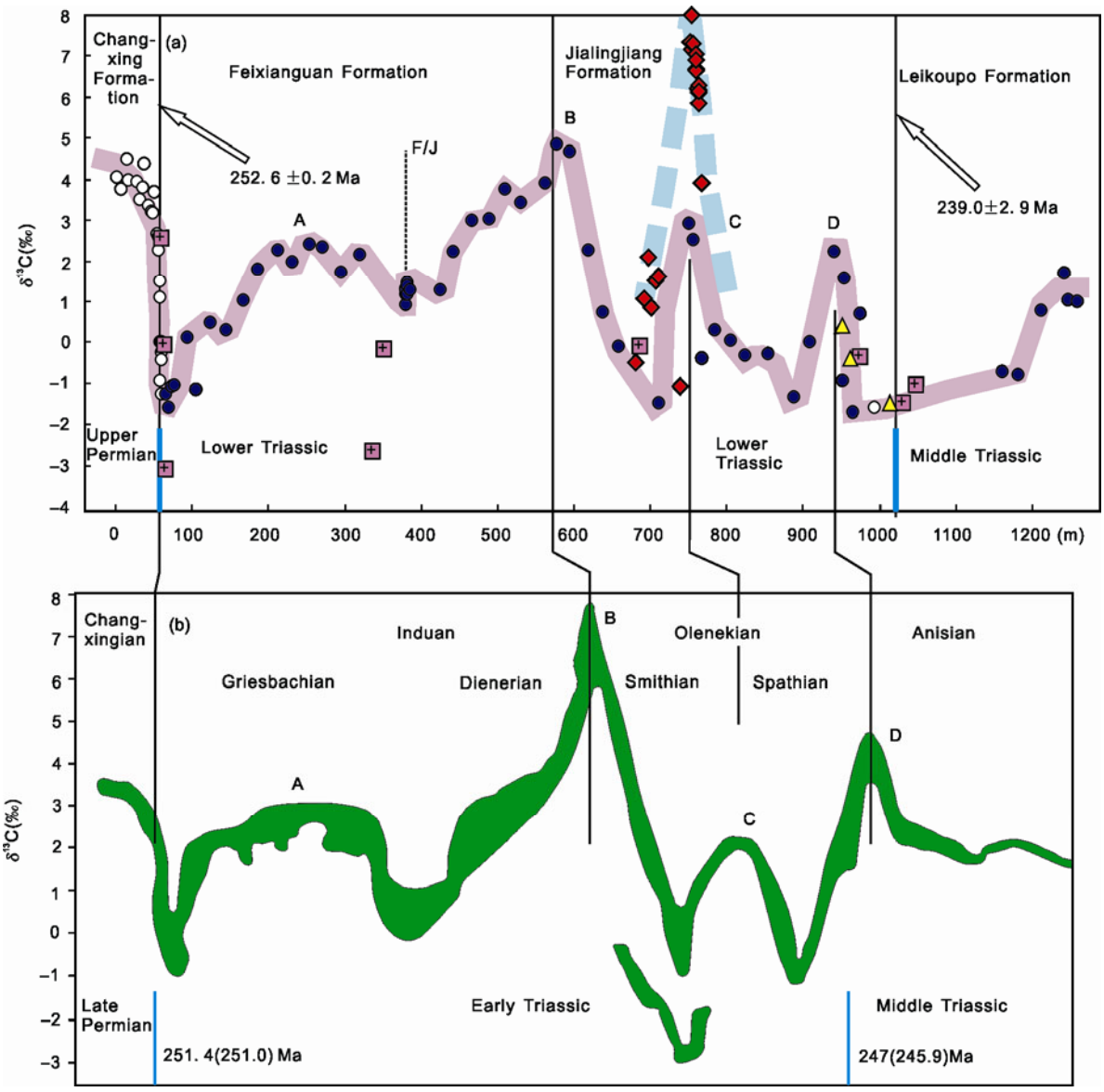

Figure 10 Comparison of the δ^{13}C isotope curve from Eastern Sichuan Basin and Guizhou Province. (a) The carbon isotope evolution curve in Late Permian-Early Triassic, Eastern Sichuan Basin. Ages of Changxing/Feixianguan Formation boundary and Jialingjiang/ Leikoupo Formation boundary are based on refs. [30, 36], respectively. Squares represent the samples with Mn/Sr ratio>2, hollow circles the samples from Zhongliang Mountain section, solid circles the samples from Yangtianwo section, rhombus the samples from Well Heba-1. For details about A, B, C, D peaks and F/J boundary see discussions in the text. (b) The carbon isotope evolution curve in Late Permian-Early Triassic, Guizhou Province (from ref. [12]). Ages are from refs. [37–40], wherein the age in parentheses is from ref. [40].

tium-isotope record from the sections at Quxian, Sichuan Province, southwestern China. Although based on the same methods as radiometric dating, an age of 247 Ma from Payne et al. [12] for the Early-Middle Triassic boundary (Figure 10(b)) is much older than that derived from Huang et al. [41]. It is suggested that those volcanic ash beds are not associated with the same age. If so, green-bean rock could not be regarded as a synchronous marker.

4.2 A correlation between the δ^{13}C curves from eastern Sichuan and Guizhou provinces

(1) In general, the Early Triassic δ^{13}C profiles originating from eastern Sichuan show comparable to those from Guizhou Province (Figure 10(a)). A sharp P-T negative δ^{13}C excursion is followed by a relatively high plateau of δ^{13}C values throughout the Early Triassic. These δ^{13}C curves exhibit four high peaks over 2‰ and three peaks coincide well with the Dienerian-Smithian, Smithian-Spathian, and Spathian-Anisian boundary, respectively (Figure 10(b)). However, the Spathian-Anisian boundary occurs earlier than the position of green-bean rock.

(2) Two Feixianguan-Jialingjiang Formation boundaries occur in Figure 10. One is marked by dash line, which represents the position identified lithologically in field. The other lies near the B peak corresponding to the Dienerian-

Smithian boundary and represents the location for the top of Feixianguan Formation according to geological map (scale: 1/50000). The former may coincide with the Griesbachian-Dienerian boundary, but no biostratigraphic evidence can be provided at present.

4.3 Explanation for the Early Triassic δ^{13}C record

For our measured sections, it does appear that apparently large and rapid carbon isotope fluctuations (in about 5 Ma, assuming 245.9 Ma as P-T boundary age and 251 Ma as Early-Middle Triassic boundary age) have occurred in the Early Triassic. Within the Early Triassic, the δ^{13}C excursions underwent a positive shift from about –2 ‰ to 8‰. Such a fluctuation was unique in Phanerozoic and was restricted in Early Triassic, and disappeared at the Early-Middle Triassic boundary. Note that prior to the P-T boundary and after the final rise within the Early Triassic, the values of δ^{13}C remain a steady state with some small-amplitude perturbations [42] (less than 2‰; Figure 11).

The Early Triassic fluctuations in δ^{13}C profiles, in principle, would result from the perturbations of the global carbon cycle, which are generally accepted as good proxies for perturbations of ecologic environments. They would also represent the effects of the mass extinction on the environmental and biotic conditions [13]. A wide variety of hypothetical processes have been offered to explain such effects. Unfortunately, there is some confusion over whether such δ^{13}C anomaly represents global trend or just a regional signature. To solve this and evaluate the causes of the positive δ^{13}C excursions, more δ^{13}C data are necessary, as discussed above. It is not the purpose of this paper to evaluate all of the many hypotheses, but to provide more evidence of profound changes in the carbon cycle during the Lower Triassic and therefore to better understand the processes responsible for this. The possible causes for the δ^{13}C anomaly considered in the present paper can be stated as below.

(1) The positive excursion of δ^{13}C indicates that large amount organic carbon was buried during the Early Triassic. The absence of coal deposition in Early Triassic suggests the organic carbon derived from terrestrial vegetation was limited, and the bacteria and algae organisms might be the essential organic carbon source. Kolber et al. [43] emphasized the contribution of bacteria and algae to the carbon cycle in the ocean and argued that bacteria could considerably modify the primary δ^{13}C of seawater. Thus, the bacteria and algae might be major primary producers for organic carbon during the Early Triassic.

(2) About 90% of all species became extinct during the Permian-Triassic extinction [1, 2], which was followed by a long survival period and a substantial biotic recovery. The long survival intervals accompanied by the massive resurgence of microbialites [44] and anachronistic facies [45], which can be recorded by some distinctive sedimentary structures such as the flat-pebble conglomerate, vermicular limestone, and stromatolites. Those structures have recently been suggested to be restricted to Proterozoic-Cambrian and therefore are regarded as anomalous for the Phanerozoic. The co-occurrence of these facies and global extinctions of marine invertebrates may also result in carbon cycle perturbations in Early Triassic.

(3) It is clear that the δ^{13}C record of the dolomites of the Jialingjiang Formation (especially the 2nd Member) from the Upper Yangtze region is unusual and characterized by massive 10‰ changes. This may cause large amounts of methane from the exogenous carbon source into the stored methane hydrates with extremely depleted δ^{13}C values.

(4) Recently, the release of methane stored in methane hydrates has been proposed to explain the P-T boundary δ^{13}C anomaly [46–48]. Dickens [48] introduced the idea that methane hydrate acts as a large capacitor in an organic carbon cycle. If this is true, the δ^{13}C rise in the Early Triassic,

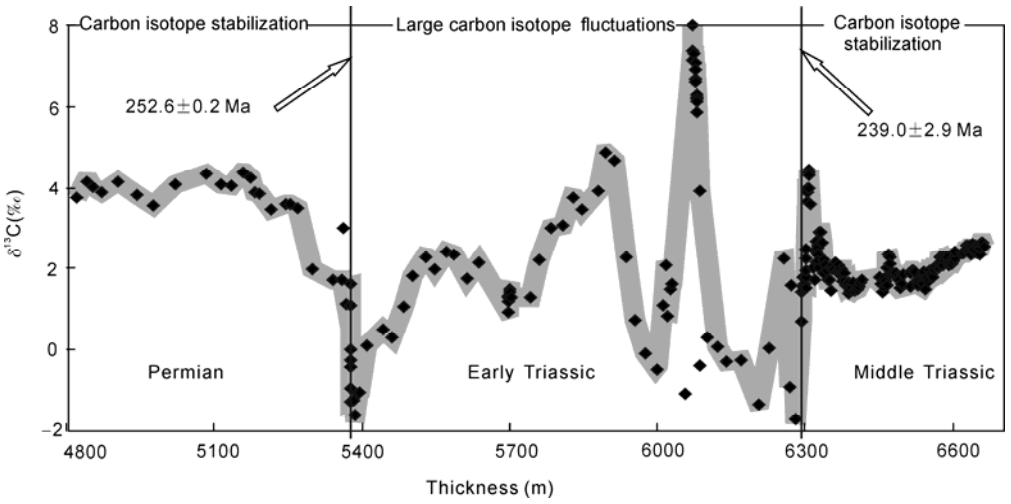

Figure 11 Carbon isotope evolution curve for marine carbonates of Permian to Middle Triassic. Data of Permian from ref. [42, 12], and the Early Triassic data are from this paper (including data from Well Heba-1). Accumulative thickness is 0 m at the boundary in different sections.

which is contrary to a $\delta^{13}C$ decline in P-T transition, may be due to a "capacitor conversion" serving from a carbon source into a carbon sink. Based on a perceived dissimilarity in the magnitude and rapidity of the $\delta^{13}C$ records from Lower to Upper Yangtze, it can be inferred that the degree of such conversion may depend on local conditions.

(5) Carbonate production depends largely on biological communities, especially marine invertebrates. Most invertebrates have been seriously affected by the mass extinction event. Thus, the Early Triassic carbonates, which were deposited after the disappearance of massive marine invertebrates, are composed dominantly of non-biological origin fragments such as oolites. In addition, the amount of terrestrial vegetation in the Early Triassic world was sharply decreased. So the Late Triassic unit is characterized by a thick succession of clastic sediments around the world [4]. This would lead to the reduction in the volumes of dissolved CO_2, which was derived from organic decomposition and released to exogenesis carbon systems. This process may also introduce substantial volumes of heavy carbon, causing the positive $\delta^{13}C$ shift. However, the mechanism that the carbonates work as a carbon cycle adjustor is problematic and still needs more quantitative works.

(6) On the basis of the discussions above, such a change of the carbon cycle would involve the amount of both marine invertebrates and carbonates. The terrestrial vegetation and the marine carbonates are two most important regulators for carbon cycle. An insufficient amount of terrestrial vegetation and the marine carbonates would appeal for rapid $\delta^{13}C$ shifts. Thus, we should develop an awareness of the need to better protect and manage the world's marine invertebrates.

5 Conclusions

(1) The marine carbonates of the Late Permian-Early Triassic in Eastern Sichuan Basin are characterized by higher Sr and lower Mn concentrations, and lower Mn/Sr ratios, which represent the original geochemistry signatures of ancient seawater. Early Triassic $\delta^{13}C$ profiles originating from Eastern Sichuan Basin and Guizhou Province show finely comparable patterns.

(2) The established carbon isotope curve in this study differs somewhat from other trends established in the Lower Yangtze region, such as Chaohu in Anhui Province.

(3) The dolomites of Jialingjiang Formation (especially T_1j^2) in the Upper Yangtze region have a very high $\delta^{13}C$ value up to 8‰, which may be related to the formation of methane. This may also demonstrate that the production of methane in marine is in favor of the precipitation of dolomite.

(4) The $\delta^{13}C$ values of marine carbonates of Early Triassic in Northeastern Sichuan Basin have the maximum fluctuating amplitude in Phanerozoic. The $\delta^{13}C$ value changed from the minimum of about –2‰ to the maximum of 8‰ in the epoch spanning about 5 Ma. Because the $\delta^{13}C$ values in Lower Yangtze region have the different fluctuation model (from the minimum of about –6‰ to the maximum of 4‰) or even do not have any fluctuation (Chaohu area in Anhui Province), global comparative studies should be considered in future research.

(5) The $\delta^{13}C$ value of marine carbonates in the Upper Yangtze region is significantly higher than the Lower Yangtze region. This indicates that, compared to the Lower Yangtze region, the Upper Yangtze region has greater amount of organic carbon burial flux and higher potential capacity of hydrocarbon generation. More opportunities may be offered for gas hydrate reservoir of Upper Yangtze region to 'recharge' after a catastrophic release.

(6) The highest $\delta^{13}C$ value and larger fluctuations of in Early Triassic seawater might be related to reduction of the amounts of global terrestrial vegetation and marine invertebrates and carbonates, and also caused by the over prosperous of bacteria, algae and the active of methanogens bacteria in marine. The formation of methane has increased substantial of $\delta^{13}C$ value of seawater, and may have caused regional anomalies of carbon isotopic. Such fluctuations were ended at Early-Middle Triassic boundary, indicating that the earth ecosystem was reconstructed and recovered.

(7) The carbon isotopic curve of Early Triassic seawater suggests that the continental vegetation and marine invertebrates are two important regulators for earth ecosystem, and play the irreplaceable roles in earth ecosystem. We should protect the marine invertebrates, especially the reefs, as well as the tropical rainforest.

We would like to express our thanks to Shi He, Li Zhiming, Fan Ming, Xu Ershe, Zhang Wentao, Hu Zuowei, Liu Haonian, Huang Peipei, Wang Qingdong, Zhang Xuehua, Tong Hongpeng, Liu Lihong, Sun Wei, Liu Tao and Wei Wenwen who participated in the fieldwork and laboratory work, and the anonymous reviewers who gave constructive suggestions that improved the paper. This work was supported by National Natural Science Foundation of China (Grant Nos. 40839908, 41172099).

1 Raup D M. Size of the Permo-Triassic bottleneck and its evolutionary implications. Science, 1979, 206: 217–218
2 Erwin D H. The Great Paleozoic Crisis: Life and Death in the Permian: Critical Moments in Paleobiology and Earth History Series. New York: Columbia University Press, 1993. 1–338
3 Korte C, Kozur H W, Bruckschen P, et al. Strontium isotope evolution of Late Permian and Triassic seawater. Geochim Cosmochim Acta, 2003, 67: 47–62
4 Veizer J, Ala D, Azmy K, et al. $^{87}Sr/^{86}Sr$, $\delta^{13}C$ and $\delta^{18}O$ evolution of phanerozoic seawater. Chem Geol, 1999, 161: 59–88
5 Tong J N, Qiu H O, Zhao L S, et al. Lower Triassic inorganic carbon isotope excursion in Chaohu, Anhui Province, China. China Univ Geosci, 2002, 13: 98–106
6 Korte C, Kozur H W, Veizer J. $\delta^{13}C$ and $\delta^{18}O$ values of Triassic brachiopods and carbonate rocks as proxies for coeval seawater and palaeotemperature. Palaeogeogr Palaeoclimatol Palaeoecol, 2005, 226: 287–306
7 Korte C, Kozur H W, Joachimski M M. et al. Carbon, sulfur, oxygen and strontium isotope records, organic geochemistry and biostrati-

graphy across the Permian/Triassic boundary in Abadeh, Iran. Int J Earth Sci, 2004, 93: 565–581
8 Korte C, Kozur H W. Carbon isotope stratigraphy across the Permian/Triassic boundary at Jolfa (NW-Iran), Peitlerkofel (Sas de Pu¨ tia, Sass de Putia), Pufels (Bula, Bulla), Tesero (all three Southern Alps, Italy) and Gerennavár (Bükk Mts., Hungary). J Alp Geol, 2005, 47: 119–135
9 Kozur H W. Integrated ammonoid, conodont and radiolarian zonation of the Triassic. Hallesches Jahrb Geowiss, 2003, 25: 49–79
10 Kozur H W. Integrated ammonoid, conodont and radiolarian zonation of the Triassic and some remarks to Stage/Substage subdivision and the numeric age of the Triassic stages. Albertiana, 2003, 28: 57–74
11 Horacek M, Brandner R, Abart R. Carbon isotope record of the P/T boundary and the Lower Triassic in the southern Alps: Evidence for rapid changes in storage of organic carbon. Palaeogeogr Palaeoclimatol Palaeoecol, 2007, 252: 347–354
12 Payne J L, Lehrmann D J, Wei J, et al. Large perturbations of the carbon cycle during recovery from the end-Permian extinction. Science, 2004, 305: 506–509
13 Zuo J X, Tong J N, Qiu H O, et al. Carbon isotope composition of the Lower Triassic marine carbonates, Lower Yangtze region, South China. Sci China Ser D-Earth Sci, 2006, 49: 225–241
14 Huang S J, Clay minerals in clay rocks near P/T boundary from Guangyuan and Chongqing, Sichuan (in Chinese). J Chengdu Univ Tech (Sci Tech Ed), 1992, 19: 66–73
15 Huang S J. Microspherulitic and clastic mineral in the clay rock near the Permian-Triassic interface of Zhongliangshan Mountain, Chongqing (in Chinese). Acta Sediment Sin, 1993, 11: 105–113
16 Huang S J. Cathodoluminescence and diagenetic alteration of marine carbonate minerals (in Chinese). Sediment Facies Palaeogeogr, 1990, 10: 9–15
17 Hu Z W, Huang S J, Qing H R, et al. Evolution and global correlation for strontium isotopic composition of marine Triassic from Huaying Mountain, eastern Sichuan. Sci China Ser D-Earth Sci, 2008, 51: 540–549
18 Huang S J, Qing H R, Huang P P, et al. Evolution of strontium isotopic composition of seawater from Late Permian to Early Triassic based on study of marine carbonates, Zhongliang Mountain, Chongqing, China. Sci China Ser D-Earth Sci, 2008, 51: 528–539
19 Brand U, Veizer J. Chemical diagenesis of multicomponent carbonate system-2: Trace elements. J Sediment Petrol, 1980, 50: 1219–1236
20 Huang S J, Qing H R, Hu Z W, et al. Cathodoluminescence and diagenesis of the carbonate rocks in Feixianguan Formation of Triassic, eastern Sichuan Basin of China (in Chinese). J China Univ Geosci, 2008, 33: 26–34
21 Walter M R, Veevers J J, Calver C R, et al. Dating the 840–544 Ma Neoproterozoic interval by isotopes of strontium, carbon, and sulfur in seawater, and some interpretative models. Precambrian Res, 2000, 100: 371–433
22 Huang S J, Wang C M, Huang P P, et al. Scientific research frontiers and considerable questions of carbonate diagenesis (in Chinese). J Chengdu Univ Tech (Sci Tech Ed), 2008, 35: 1–10
23 Derry L A, Keto L, Jacobsen S, et al. Sr isotopic variations in Upper Proterozoic carbonates from Svalbard and east Greenland. Geochim Cosmo Acta, 1989, 53: 2331–2339
24 Kaufman A J, Jacobsen S B, Knoll A H. The Vendian record of Sr- and C-isotopic variations in seawater: implications for tectonics and paleoclimate. Earth Planet Sci Lett, 1993, 120: 409–430
25 Kaufman A J, Knoll A H, Awramik S M. Biostratigraphic and chemostratigraphic correlation of Neoproterozoic sedimentary successions: Upper Tindir Group, northwestern Canada, as a test case. Geology, 1992, 20: 181–185
26 Huang S J, Carbonate Diagenesis (in Chinese). Beijing: Geological Publishing House, 2010. 103–114
27 Magaritz M, Anderson R Y, William T, et al. Isotope shifts in the Late Permian of the Delaware Basin, Texas, precisely timed by varved sediments. Earth Planet Sci Lett, 1983, 66: 111–124
28 Huang S J, Huang Y, Lan Y F, et al. A comparative study on strontium isotope composition of dolomites and their coeval seawater in the late Permian-early Triassic, NE Sichuan Basin (in Chinese). Acta Petro Sin, 2011, 27: 3831–3842
29 Huang S J, Huang K K, Li Z M, et al. The calcite cement as a by-product of thermochemical sulfate reduction in Triassic dolomite, NE Sichuan Basin, China. J Earth Sci, 2012, 23: 88–96
30 Mundil R, Ludwig K R, Metcalfe L, et al. Age and Timing of the Permian mass extinctions: U/Pb dating of closed-system zircons. Science, 2004, 305: 1760–1763
31 Claoue-Long J C, Zhang Z C, Ma G G, et al. The age of the Permian-Triassic boundary. Earth Planet Sci Lett, 1991, 105: 182–190
32 Chen J S, Shao M R, Huo W G, et al. Carbon isotope of carbonate strata at Permian-Triassic boundary in Changxing, ZheJiang (in Chinese). Chin J Geol, 1984, 19: 88–93
33 Magarita M, Bar R, Baud A, et al. The carbon isotope shift at the Permian-Triassic boundary in the Southern Alps is gradual. Nature, 1988, 331: 337–389
34 Holser W T, Magaritz M. Events near the Permian-Triassic boundary. Modern Geol, 1987, 11: 155–180
35 Huang S J. Carbon isotopes of Permian and Permian-Triassic boundary in Upper Yangtze platform and the mass extinction (in Chinese). Geochemica, 1994, 23: 60–67
36 Wang Y B, Liu G Y, Yao J X, et al. Age determination of the Lower-Middle Triassic boundary at Ganheqiao, Wangmo, Guizhou Province (in Chinese). Acta Geol Sin, 2004, 78: 587–590
37 Bowring S A, Erwin D H, Jin Y G, et al. U/Pb zircon geochronology and Tempo of the End-Permian mass extinction. Science, 1998, 280: 1039–1045
38 Martin M W, Lehrmann D J, Bowring S A, et al. Timing of Lower Triassic carbonate bank buildup and biotic recovery following the end-Permian extinction across the Nanpanjiang Basin, South China. Ann Meeting Geol Soc Am, 2001, 33: 201
39 Mundil R, Brack P, Meier M, et al. High resolution U-Pb dating of Middle Triassic volcaniclastics: Time-scale calibration and verification of tuning parameters for carbonate sedimentation. Earth Planet Sci Lett, 1996, 141: 137–151
40 Zhang S G, Zhang Y B, Yan H J. A brief introduction to the "International Stratigraphic Chart" (2008) (in Chinese). J Stratigra, 2009, 33: 1–10
41 Huang S J, Pei C R, Qing H R, et al. Age calibration for the boundary between Lower and Middle Triassic by strontium isotope stratigraphy in eastern Sichuan (in Chinese). Acta Geol Sin, 2006, 80: 1691–1698
42 Huang S J. A study on carbon and strontium isotopes of Late Palaeozoic marine carbonates in the Upper Yangtze platform, southwest China (in Chinese). Acta Geol Sin, 1997, 71: 45–53
43 Kolber Z S, Plumley F G, Lang A S, et al. Contribution of aerobic photoheterotrophic bacteria to the carbon cycle in the ocean. Science, 2001, 292: 2492–2495
44 Huang S J. Vermicular limestone and its origin (in Chinese). J Chengdu Univ Tech (Sci Tech Ed), 1984, 11: 60–67
45 Zhao X M, Tong J N, Yao H Z, et al. Anachronistic facies in the Lower Triassic of South China and their implications to the ecosystems during the recovery time. Sci China Ser D-Earth Sci, 2008, 51: 1646–1657
46 Retallack G L. Postapocalyptic greenhouse paleoclimate revealed by earliest Triassic paleosols in the Sydney Basin, Australia. Geol Soc Am Bull, 1999, 111: 52–70
47 Krull E S, Retallack G J. δ^{13}C depth profiles from paleosols across the Permian-Triassic boundary: Evidence for methane release. Geol Soc Am Bull, 2000, 112: 1459–1472
48 Dickens G R. Rethinking the global carbon cycle with a large, dynamic and microbially mediated gas hydrate capacitor. Earth Planet Sci Lett, 2003, 213: 169–183